6. SAFETY AND ENVIRONMENT

Thomas J. Dolan Jeffrey Crowell Hesham Y. Khater

Contents

6. SAFETY AND ENVIRONMENT

6.1. INTRODUCTION

While the scope of the SPPS did not permit a thorough investigation of the safety and environmental characteristics of the SPPS/MHH, several issues were examined. The main safety and environmental aspects considered for the SPPS/MHH are: (1) Routine release of tritium, (2) Safety precautions with lithium, (3) Accidental release of radioisotopes driven by a lithium fire, (4) Accidental release of vanadium pentoxide (toxicity), and (5) Waste disposal.

The tritium inventory and routine release rate are not estimated here. The release rate can probably be kept within the desired limits (~20 GBq/s) by using standard techniques for tritium removal from liquid metals, such as cold trapping and molten salt extraction.

Some advantages of using a lithium breeder and coolant are: (1) Li is a low-activation breeder material, (2) It provides a satisfactory breeding ratio, *i.e.,* Be is not required, and Be toxicity can be avoided; (3) Li blankets have a low coolant pressure specially if insulating material is used. As such, ruptures of tubes and welds are less likely, (4) Li blankets operates at a high temperature operation. The resultant high energy conversion efficiency reduces the amount of heat rejected to the environment; (5) Natural convection removal of decay heat is possible because of good coolant properties (reasonable viscosity, specific heat comparable to that of water, and thermal conductivity about 90 times higher than water)

The main hazard associated with lithium is chemical reactivity. The energy release associated with a lithium fire could heat the vanadium alloy structure, increasing the mobilization rates of radioisotopes. The average energy release from reaction of lithium with air (N and O) was estimated to be about 12.3 MJ/kg(Li) [1]. Vanadium can also react with oxygen, releasing 12.8 MJ/kg(V), but the oxidation rate is very slow.

6.2. SAFETY PRECAUTIONS WITH LITHIUM

In order to promote safe use of lithium in the stellarator power plant, several safety precautions are recommended:

- Use a low-afterheat structural material such as V-5Cr-5Ti.
- Minimize the fire hazard by minimizing the mass of lithium in the system. This can be accomplished by placing the intermediate heat exchanger close to the torus and using a low volume fraction of lithium in the shield.
- Use three barriers between the lithium and the air. coolant ducts vacuum chamber around coolant ducts, and a stainless steel shell on ducts that are outside of the vacuum chamber reactor hall with a steel liner to prevent lithium contact with concrete.
- Use an inert cover gas (such as argon) around the torus. Keep argon out of high neutron flux areas, to avoid its activation.
- Exclude water from the reactor hall.
- If liquid metal is used for the intermediate coolant loop, use double-walled steam generator tubes. Double-wall tube steam generator technology has been successfully demonstrated in the EBR-II reactor [1, 2].
- Place drain tanks below the torus, so that the lithium can be quickly drained during an accident to prevent exposure to air. The tanks would contain argon sealed by fire-retardant valves [1].
- Put most other lithium piping connections above the torus, so that leaks in those tubes will not accidentally drain the torus.
- The floors should slope so that spilled lithium will flow along the stainless steel liner to drains.
- Use an inert powder (such as hollow graphite microspheres) to cover lithium spills. The powder would float on top of the lithium, minimizing contact with the air in the event that the argon cover gas were lost.
- Avoid missile impacts on the lithium coolant system by placing turbine generators away, oriented to avoid missiles traveling towards the torus. Reduce aircraft impact consequences by locating the torus below grade inside a concrete dome.

6.3. ACCIDENTAL RELEASE OF RADIOISOTOPES

The energy sources present in the power plant are listed in Table 6.3-I. The fractional vanadium oxidation is based on the hypothetical accident sequenced described below. The chemical energy of the lithium is dominant.

The "worst-case" accident scenario considered here is the rupture of a lithium duct, failure of the drain system, breach of the reactor hall allowing air ingress, and complete burning of all the lithium. Such a pessimistic scenario is required for an ESECOM-type analysis. It is used here for two reasons: (1) This type of analysis is needed to facilitate comparison with previous studies, such as ESECOM, ARIES, and PULSAR; and (2) A probabilistic regulatory-type analysis would require more resources and failure-rate data than are available.

As for the ESECOM V/Li power plant, it is assumed that the first wall/blanket reaches 1573 K for 10 hours, followed by 1273 K for 40 hours. (This case was also used for the ARIES-II tokamak analysis.) All mobilized material is assumed to reach the site

Table 6.3-I.
Some Energy Sources in the SPPS/MHH Power Plant

Source	Energy (GJ)
Plasma magnetic energy	negligible[(a)]
Plasma thermal energy	0.54
Chemical energy of 0.12% V oxidation[(b)]	4
Magnetic energy stored in the coils	78
Decay heat energy (7 days)	1,940
Chemical energy of lithium fire[(b)]	3,500

[(a)] Because of negligible plasma current.

[(b)] For 42 m^3 of V.

[(c)] For 600 m^3 of Li.

boundary. No credit is taken for containment, plate-out, or deposition. Such a pessimistic scenario would not be used for a regulatory-type analysis.

In estimating the potential off-site radiation dose, the following pessimistic conditions are assumed: (1) 1-km site boundary radius; (2) 1 m/s wind velocity; (3) Pasquill F stability conditions; and (4) near-ground-level release (0–10 m).

For these conditions a table of "effective dose" conversion factors derived with the MELCOR Accident Consequence Code System (MACCS) [1] is used to estimate the off-site dose to a Maximum Exposed Individual that could result from release of each isotope. The activities of about 400 radioactive isotopes present in the first wall, blanket, and shield are considered. Mobilization fractions are estimated for some of the most important elements, based upon INEL experimental data, assuming as was done for the ARIES-II study [1]. Default mobilization fractions for the remaining elements are taken from Ref. [1]. The dominant isotopes and resulting potential off-site doses to a Maximum Exposed Individual are listed in Table 6.3-II to 6.3-V.

Table 6.3-II.
Estimated Doses at the Site Boundary 10 Minutes after a Worst-Case Accident (First-Wall Contribution$^{(a)}$)

	Activity (PBq)	Mobilization Fraction	Conversion Factor (Sv/TBq)	Effective Dose (Sv)
^{24}Na	$1.81 \times 10^{+0}$	$1.00 \times 10^{+0}$	4.62×10^{-4}	0.8379
^{48}Sc	$4.30 \times 10^{+2}$	3.52×10^{-4}	1.15×10^{-3}	0.1737
T	$1.39 \times 10^{+1}$	$1.00 \times 10^{+0}$	2.38×10^{-6}	0.0329
^{46}Sc	$4.18 \times 10^{+1}$	3.52×10^{-4}	2.22×10^{-3}	0.0327
^{45}Ca	$2.97 \times 10^{+1}$	5.25×10^{-3}	6.96×10^{-5}	0.0108
^{32}P	6.45×10^{-1}	3.00×10^{-1}	5.15×10^{-5}	0.0100
Total:				1.14

(a) For a first-wall volume of 13.6 m^3.

Table 6.3-III.
Estimated Doses at the Site Boundary 10 Minutes after a Worst-Case Accident (Blanket Contribution[(a)])

	Activity (PBq)	Mobilization Fraction	Conversion Factor (Sv/TBq)	Effective Dose (Sv)
^{24}Na	$6.75 \times 10^{+0}$	$1.00 \times 10^{+0}$	4.62×10^{-4}	$3.12 \times 10^{+0}$
^{48}Sc	$1.50 \times 10^{+3}$	1.02×10^{-4}	1.15×10^{-3}	1.75×10^{-1}
T	$4.59 \times 10^{+1}$	$1.00 \times 10^{+0}$	2.38×10^{-6}	1.09×10^{-1}
^{32}P	$2.85 \times 10^{+0}$	3.00×10^{-1}	5.15×10^{-5}	4.40×10^{-2}
^{182}Ta	$2.19 \times 10^{+0}$	1.00×10^{-2}	1.66×10^{-3}	3.64×10^{-2}
^{46}Sc	$1.57 \times 10^{+2}$	1.02×10^{-4}	2.22×10^{-3}	3.55×10^{-2}
^{74}As	9.67×10^{-2}	3.00×10^{-1}	7.80×10^{-4}	2.26×10^{-2}
^{76}As	5.62×10^{-1}	3.00×10^{-1}	1.30×10^{-4}	2.19×10^{-2}
^{99}Mo	2.58×10^{-1}	3.00×10^{-1}	1.74×10^{-4}	1.35×10^{-2}
^{35}S	$4.03 \times 10^{+0}$	$1.00 \times 10^{+0}$	3.12×10^{-6}	1.26×10^{-2}
^{51}Cr	$1.06 \times 10^{+3}$	2.43×10^{-4}	3.53×10^{-5}	9.10×10^{-3}
^{49}V	$9.70 \times 10^{+2}$	1.54×10^{-3}	3.61×10^{-6}	5.40×10^{-3}
^{47}Sc	$4.73 \times 10^{+2}$	1.02×10^{-4}	8.61×10^{-5}	4.15×10^{-3}
^{75}Se	2.10×10^{-2}	3.00×10^{-1}	5.18×10^{-4}	3.26×10^{-3}
^{45}Ca	$9.99 \times 10^{+1}$	4.22×10^{-4}	6.96×10^{-5}	2.93×10^{-3}
^{58}Co	1.73×10^{-1}	1.00×10^{-2}	1.08×10^{-3}	1.87×10^{-3}
^{47}Ca	$3.56 \times 10^{+0}$	4.22×10^{-4}	7.08×10^{-4}	1.06×10^{-3}
Total:				3.63

(a) For a blanket volume of 374 m^3.

Table 6.3-IV.
Estimated Doses at the Site Boundary 10 Minutes after a Worst-Case Accident (Hot Shield Contribution[(a)])

	Activity (PBq)	Mobilization Fraction	Conversion Factor (Sv/TBq)	Effective Dose (Sv)
^{24}Na	$2.99 \times 10^{+0}$	$1.00 \times 10^{+0}$	4.62×10^{-4}	$1.38 \times 10^{+0}$
^{54}Mn	$9.49 \times 10^{+3}$	1.16×10^{-4}	9.19×10^{-4}	$1.01 \times 10^{+0}$
^{56}Mn	$9.11 \times 10^{+4}$	1.16×10^{-4}	3.33×10^{-5}	3.51×10^{-1}
^{182}Ta	$1.83 \times 10^{+1}$	1.00×10^{-2}	1.66×10^{-3}	3.05×10^{-1}
^{210}Po	2.15×10^{-2}	1.00×10^{-1}	9.07×10^{-2}	1.95×10^{-1}
^{188}Re	$2.14 \times 10^{+1}$	3.00×10^{-1}	2.65×10^{-5}	1.70×10^{-1}
^{124}Sb	$2.47 \times 10^{+0}$	3.00×10^{-2}	1.98×10^{-3}	1.46×10^{-1}
^{160}Tb	$7.06 \times 10^{+0}$	1.00×10^{-2}	1.26×10^{-3}	8.92×10^{-2}
^{45}Ca	$1.08 \times 10^{+1}$	1.00×10^{-1}	6.96×10^{-5}	7.50×10^{-2}
^{122}Sb	$4.98 \times 10^{+0}$	3.00×10^{-2}	2.62×10^{-4}	3.92×10^{-2}
^{60}Co	$1.05 \times 10^{+2}$	2.54×10^{-5}	4.55×10^{-3}	1.22×10^{-2}
^{110m}Ag	$1.01 \times 10^{+0}$	1.00×10^{-2}	3.54×10^{-3}	3.59×10^{-2}
^{113m}Cd	8.05×10^{-2}	1.00×10^{-1}	4.14×10^{-3}	3.33×10^{-2}
^{76}As	8.22×10^{-1}	3.00×10^{-1}	1.30×10^{-4}	3.21×10^{-2}
T	$1.34 \times 10^{+1}$	$1.00 \times 10^{+0}$	2.38×10^{-6}	3.19×10^{-2}
^{32}P	$7.27 \times 10^{+0}$	2.54×10^{-2}	5.15×10^{-5}	9.53×10^{-3}
^{47}Ca	3.58×10^{-1}	1.00×10^{-1}	7.08×10^{-4}	2.53×10^{-2}
^{48}Sc	$1.66 \times 10^{+2}$	3.40×10^{-5}	1.15×10^{-3}	6.46×10^{-3}
^{186}Re	9.35×10^{-1}	3.00×10^{-1}	4.26×10^{-5}	1.20×10^{-2}
^{51}Cr	$3.88 \times 10^{+3}$	2.57×10^{-5}	3.53×10^{-5}	3.52×10^{-3}
^{192}Ir	8.75×10^{-1}	1.00×10^{-2}	1.14×10^{-3}	1.00×10^{-2}
^{192m}Ir	9.96×10^{-2}	1.00×10^{-2}	5.87×10^{-3}	5.85×10^{-3}
Total:				2.66

(*a*) For a hot shield volume of 587 m^3.

Table 6.3-V.
Estimated Doses at the Site Boundary 10 Minutes after a Worst-Case Accident (Low-Temperature Shield Contribution[(a)])

	Activity (PBq)	Mobilization Fraction	Conversion Factor (Sv/TBq)	Effective Dose (Sv)
T	$8.61 \times 10^{+0}$	$1.00 \times 10^{+0}$	2.38×10^{-6}	0.0205
^{56}Mn	$1.11 \times 10^{+3}$	3.74×10^{-4}	3.33×10^{-5}	0.0138
^{54}Mn	$1.59 \times 10^{+1}$	3.74×10^{-4}	9.19×10^{-4}	0.0055
^{210}Po	3.82×10^{-4}	1.00×10^{-1}	9.07×10^{-2}	0.0035
^{182}Ta	1.77×10^{-1}	1.00×10^{-2}	1.66×10^{-3}	0.0029
^{160*}Tb	1.70×10^{-1}	1.00×10^{-2}	1.26×10^{-3}	0.0022
^{124}Sb	2.93×10^{-2}	3.00×10^{-2}	1.98×10^{-3}	0.0017
Total:				0.050

(*a*) For a low-temperature shield volume of 538 m^3.

The dominant isotopes are ^{54}Mn in the shield and ^{24}Na in the blanket. A recent estimate shows that practically all of the Na could be mobilized at 1573 K [1]. From this analysis, the total Effective Dose (based on MACCS dose conversion factors) would be about 7.5 Sv, exceeding the 2 Sv threshold dose for prompt off-site fatalities.

The ESECOM and ARIES studies used the older Porter dose conversion factors. With the Porter dose conversion factors, the off-site Early Dose would be about 1 Sv. It might be appropriate to consider this lower value when comparing the SPPS with those power plants.

There are many mitigating factors that would reduce the off-site dose below the value of the pessimistic case considered here. The high temperatures and oxidation leading to radioactivity releases would be prevented or reduced by many barriers, passive safety features, and phenomena. These include the chamber, reactor hall, lithium drains, inert gas, fire suppression system, building integrity, aerosol plate out in the building, stack, and aerosol settling outside. The approximate effectiveness of some of these safety features is indicated in Table 6.3-VI.

Table 6.3-VI.
Effectiveness of Some Fusion Power Plant Safety Features[(a,b)]

Design Features	
No water in building	Water ingress would require breach of the confinement plus a source of water.
Low pressure coolant	Coolant pressurization would require a pressure source, such as a chemical reaction, combined with intact ducts (or very small leaks).
Passive Features	**Typical failure rates**
Multiple barriers	
Vessels & ducts	10^{-4}–10^{-5}/y for strong vessels
Shell	10^{-1}–10^{-2}/demand, weak barriers
Building	10^{-1}/demand
Lithium drains to tanks	10^{-1}–10^{-2}/demand
Concrete liner	10^{-3}/demand
Inert cover gas	10^{-1}/demand
Stack structure	10^{-4}–10^{-5}/y for earthquakes
Aerosol plate-out	∼0.01%–100% releasable
Active Features	
Stack exhaust	10^{-4}–10^{-5}/h fan failure
Li fire suppression system	10^{-2}–10^{-3}/demand
Air filtration	10^{-5}/hour failure of filter fibers

(*a*)Based on information provided by L. C. Cadwallader, INEL.

(*b*)These approximate values are for illustrative purposes only, and should not be used for quantitative risk analyses.

From these values, it is apparent that, if common mode failures do not occur, the combination of all these safety features will result in very low frequencies for severe accidents.

6.4. VANADIUM RELEASE

During a high-temperature lithium fire, some of the vanadium alloy would become oxidized and mobilized as a V_2O_5 aerosol. Since vanadium is mildly toxic, the release of this aerosol to the site boundary could result in adverse health effects. Symptoms of acute vanadium exposure include respiratory tract irritation, bronchitis, and pneumonitis. Severe vanadium toxicity may also cause gastrointestinal disturbance, liver, kidney and central nervous system effects, pulmonary edema, and pneumonia. Recovery usually occurs with cessation of exposure, but sensitization may occur in previously exposed individuals. The purpose of this section is to assess the magnitude of the vanadium toxicity hazard.

There are about 250 tonnes of vanadium alloy in the stellarator power plant. The inert cover gas system would suppress oxidation of lithium and vanadium during an accident. However, if the building and chamber were breached, then oxidation of the Li and part of the V could occur. After an air ingress the lithium would tend to oxidize much faster than the vanadium, gradually raising the temperature of the first wall, blanket, and shield. The vanadium mobilization fraction for the first wall and blanket is estimated to be about 0.0012. Thus, a total of about 300 kg of V could be mobilized as V_2O_5 in a severe accident. What would the health effects be at the site boundary?

Consider a pessimistic case with release of all 300 kg during 10 hours as a very fine aerosol, with no plate-out or settling. Near-ground-level release is assumed, together with Pasquill class E or F stability, a steady wind speed $u = 1$ m/s, and a dispersion factor

$$uc/Q \;=\; 3 \times 10^{-4}\ \mathrm{m}^{-2}\,, \tag{6.4-1}$$

which is between the value from Eisenbud (6×10^{-4} m^{-2}) and the value from Porter (3.5×10^{-5} m^{-2}). The resulting average air concentration of V_2O_5 downwind at the 1 km site boundary would be

$$c \;=\; 2.5\ \mathrm{mg(V)/m^3}. \tag{6.4-2}$$

The actual concentration would probably be lower than this value, due to deposition and more favorable atmospheric conditions.) The National Institute of Safety and Health

(NIOSH) recommended threshold exposure limit to vanadium compounds in air (chronic exposure) is 0.05 mg/m^3. The concentration "Immediately Dangerous to Life and Health" (IDLH) is 70 mg/m^3. Thus, if a large lithium-vanadium fire occurred with breach of the reactor building, the chemical toxicity hazard during plume passage would be below the value that poses an immediate threat to life and health, but possibly above the value recommended for continuous, long-term exposure.

6.5. WASTE DISPOSAL

The shield materials have been selected primarily for their neutron attenuation capability and cost. A secondary consideration is the generation and disposal of long-lived radioactive wastes.

The choice of vanadium alloy with lithium coolant is particularly beneficial from the waste disposal standpoint. The lithium coolant will be continually purified during operation, and it can be recycled when the power plant is decommissioned.

The vanadium alloy will become highly radioactive during operation, but it, too, has recycle potential. If the alloy constituents were initially very pure, then the dominant radioisotopes left after tens of years cooling are ^{42}Ar (32.9 y) and its daughter product ^{42}K (12.4 h). These isotopes can be removed by remelting the alloy in vacuum. The residual activity depends upon activation of impurities initially present in the vanadium alloy, such as cobalt. In principle, with effective initial purification, the activated impurity dose rate after 20–60 years of cooling would be < 10 mSv/h, which is low enough for hands-on recycling. Such recycling would save space in waste repositories, save money by avoiding purchase of new vanadium alloy, help prevent vanadium price escalation, and help gain public acceptance of fusion power.

The steel of the shield might be recycled for shielding material in subsequent fusion power plants, or it could be disposed as waste. The low-temperature shield qualifies for Class C according to both NRC and Fetter limits. On the other hand, the high-temperature shield qualifies for Class C only according to the NRC limits.

6.6. ACTIVATION ANALYSES

6.6.1. Introduction

The safety characteristics of fusion power plants would most probably be dependent on the choice of the structural material. The level of radioactivity induced in any structure depends on the constituent elements of the irradiated material, level of neutron flux and time of irradiation. Low activation materials (LAMs) are an attractive choice because they result in lower levels of off-site doses in case of accidental release of their radioactive inventories during an accident. LAMs can also facilitate better waste management at the end of the plant life.

Detailed activation analyses were performed to identify the safety, environmental and rad-waste characteristics of the SPPS/MHH plant. The SPPS/MHH structure is made of vanadium alloy and cooled with liquid lithium.

The activity, decay heat and biological hazard potential (BHP) were calculated for up to 1000 years following shutdown. Such an evaluation of the structure activity and biological hazard potential is needed to evaluate the potential impact of radioactive inventory release at the onset of an accident. Results of the decay heat calculation are used to examine the thermal response of the fusion power core structure following a loss of coolant accident (LOCA) and/or a loss of flow accident (LOFA). The waste disposal ratings (WDR) of the fusion core structure at the end of its lifetime were also evaluated. The waste disposal rating is needed to determine if a given structure would satisfy the regulatory criteria for shallow land burial as low level waste (LLW). Finally, to assess the possibility of hands-on maintenance, contact dose rates were calculated at selected locations inside the containment building.

6.6.2. Calculational Procedure

The one-dimensional discrete ordinates neutron transport code ONEDANT [9] was used to calculate the neutron flux for the activation analysis. A 46-group neutron and 21-group gamma coupled cross section library containing P_3 Legendre expansions of the scattering cross sections based on the ENDF/B-V basic data files was used in the transport calculations. The SPPS/MHH peak and average neutron wall loadings are 2 and 1.3 MW/m^2, respectively.

The SPPS/MHH activation calculation was conducted using the DKR-ICF computer code [10] with activation cross sections taken from the new USACT93 [11]. The USACT93

library was developed by Dr. Fred Mann of Hanford Engineering Design Laboratory. It is based on neutron transmutation cross section and isotopic radioactive decay data from the ENDF/B-VI and EAF3 files. The neutron transmutation data used is in a 46-group structure format. The gamma source data is taken from the table of isotopes [12] and is in a 21-group structure format.

The structure activation results were utilized in the rad-waste classification performed using the WDR [13] computer code. The DOSE code [10] was used to calculate the contact doses behind the first wall, blanket, and high and low-temperature shields. Finally, the structure activation results were used in the off-site dose calculations presented in this chapter. The materials used in the blankets and shield are presented in Table 6.6-I. The elemental compositions of the vanadium alloy (V-5Cr-5Ti) and the low activation austenitic steel (Tenelon) are taken from the Blanket Comparison and Selection Study (BCSS) report [14]. The power plant is assumed to operate continuously for 30 full power years (FPY) which corresponds to 40 years of operation at 75% availability. The SPPS/MHH was assumed to have a 28 m diameter.

6.6.3. Structure Activity, Decay Heat, and Biological Hazard Potential

The activity induced in the blanket at the end of its lifetime is higher than the activity induced in the shield after 30 full power years. At shutdown, the blanket and shield activities are 683 MCi and 3908 MCi, respectively. Figure 6.6-1 shows the total activity induced in the different regions of SPPS/MHH as a function of time following shutdown. The blanket activity drops to 139 and 91 MCi within the first day and the first week following shutdown, respectively. One year after shutdown the blanket activity

Table 6.6-I.
Materials Used in the SPPS/MHH Analysis

First Wall	28.6% V-5Cr-5Ti,	71.4% Li	
Blanket	10% V-5Cr-5Ti,	90% Li	
Hot shield	15% V-5Cr-5Ti,	5% Li,	80% Tenelon
Low-temperature shield	15% V-5Cr-5Ti,	5% Li,	80% Borated-Tenelon

drops to 22.3 MCi compared to 505 MCi for the shield. The high-temperature shield dominates the activities induced in the SPPS/MHH shield.

The blanket short-term activity is dominated by ^{48}Sc ($T_{1/2}$ = 43.7 hr), ^{51}Cr ($T_{1/2}$ = 27.7 day), ^{47}Sc ($T_{1/2}$ = 3.349 day), and ^{45}Ca ($T_{1/2}$ = 162.7 day). On the other hand, the shield short-term activity after shutdown ($\leq$1 day) is dominated by ^{51}Cr, ^{54}Mn ($T_{1/2}$ = 312 day), ^{56}Mn ($T_{1/2}$ = 2.578 hr), and ^{187}W ($T_{1/2}$ = 23.9 hr). In the period between 1 day and 1 year after shutdown, ^{54}Mn, ^{60}Co ($T_{1/2}$ = 5.27 yr), and ^{3}H ($T_{1/2}$ = 12.3 yr) dominate the activity induced in the shield. During the same period of time, the blanket activity is dominated by ^{49}V ($T_{1/2}$ = 337 day), ^{45}Ca, and ^{46}Sc ($T_{1/2}$ = 83.81 day). Finally, the long-term activities induced in both the shield and blanket come from the steel components and are dominated by ^{14}C ($T_{1/2}$ = 5730 yr), ^{93m}Nb ($T_{1/2}$ = 16.1 yr), ^{94}Nb ($T_{1/2} = 2 \times 10^4$ yr), and ^{93}Mo ($T_{1/2} = 3.5 \times 10^3$ yr).

The temporal variation of the decay heat generated in the blanket and shield are shown in Figure 6.6-2. The total decay heat generated in the blanket at shutdown is 7.9 MW and drops to 1.2 MW within an hour and to only 0.2 MW within one week. At shutdown, 46.6 MW of decay heat are generated in the shield. The decay heat drops to only 1.71 MW within a day and 0.77 MW within the first year.

The decay heat generated in the SPPS/MHH is almost dominated by the same isotopes that dominate the level of activity. The short-term decay heat generated in the blanket is due to ^{48}Sc and ^{52}V ($T_{1/2}$ = 3.76 min). ^{46}Sc and ^{49}V are the dominant nuclides up to one year following the shutdown. ^{94}Nb and ^{14}C dominate the decay heat generated in the blanket several hundred years following the end of its lifetime. In the shield case, ^{56}Mn and ^{52}V produce most of the decay heat generated within the first 8 hours. Within the first year after shutdown, ^{56}Mn and ^{60}Co are the major sources of decay heat. The long-term decay heat is governed by the decay of ^{94}Nb and ^{108m}Ag ($T_{1/2}$ = 130 yr).

Figure 6.6-3 shows the total integrated decay heat generated in the different regions of the SPPS/MHH. One week after shutdown, the values of the integrated decay heat are 333 GJ for the blanket and 1,605 GJ for the shield. These results are useful for predicting the thermal response of the blanket and shield to a LOCA and/or LOFA.

The biological hazard potentials were calculated using the maximum permissible concentration limits in air for the different isotopes according to the NRC regulations specified in 10CFR20 [15]. Figure 6.6-4 shows the biological hazard potentials in air as a function of time following shutdown for the blanket and shield. The total BHP in the blanket at shutdown is 469×10^6 km^3. On the other hand, the total BHP generated in the shield at shutdown is 492×10^6 km^3 air.

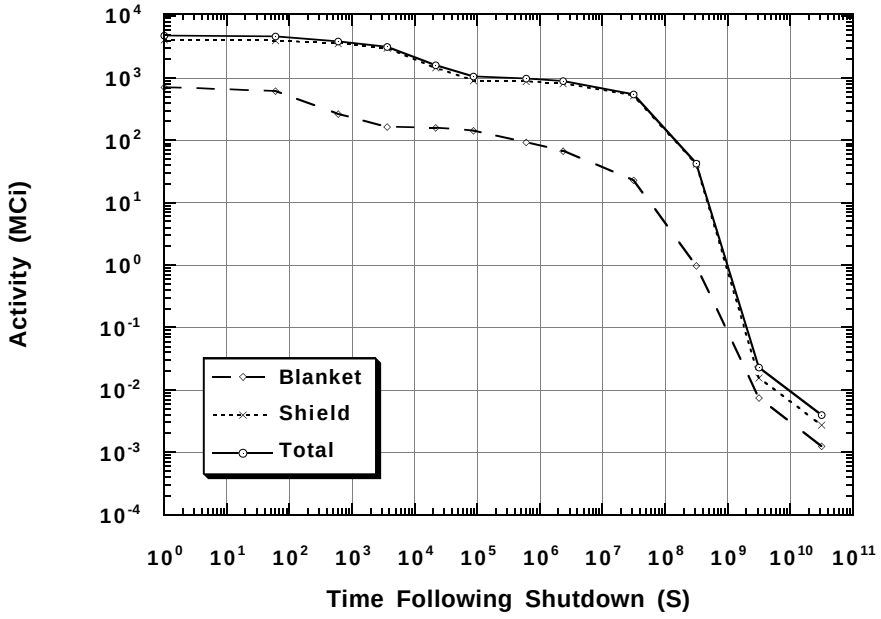

Figure 6.6-1. Activity induced in the SPPS/MHH.

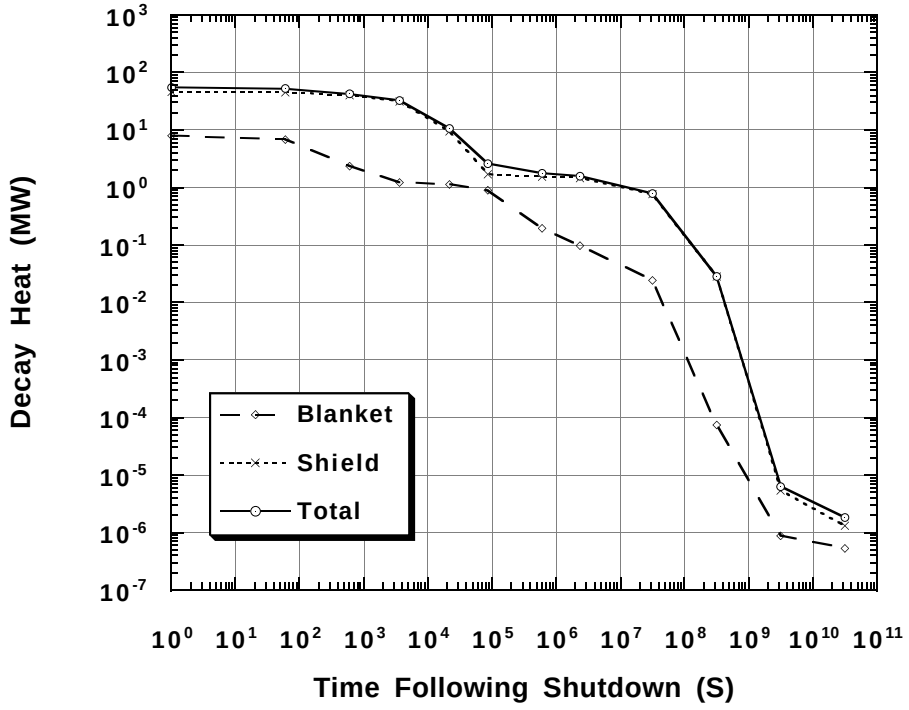

Figure 6.6-2. Decay heat induced in the SPPS/MHH.

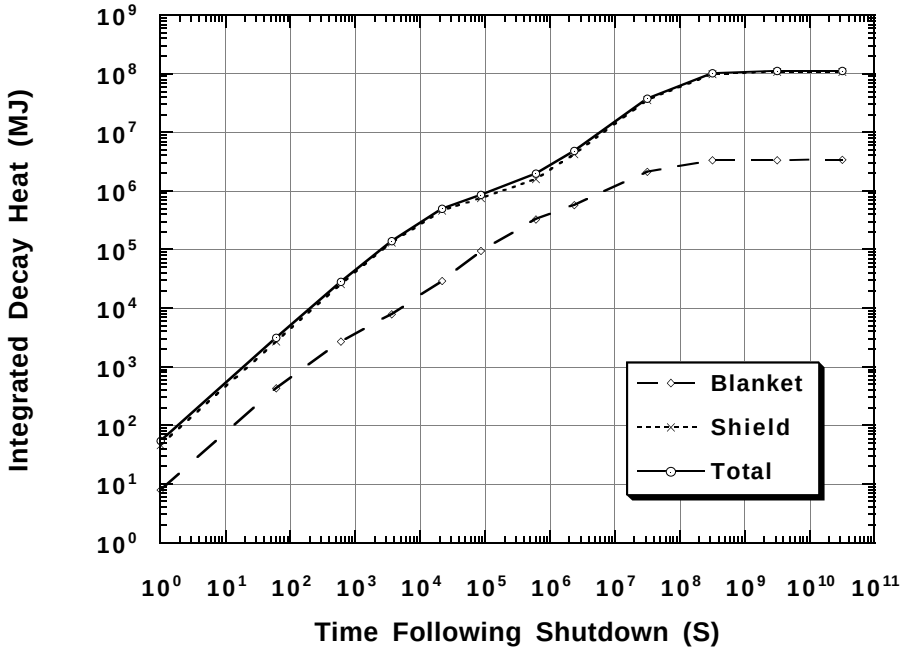

Figure 6.6-3. Integrated decay heat in the SPPS/MHH.

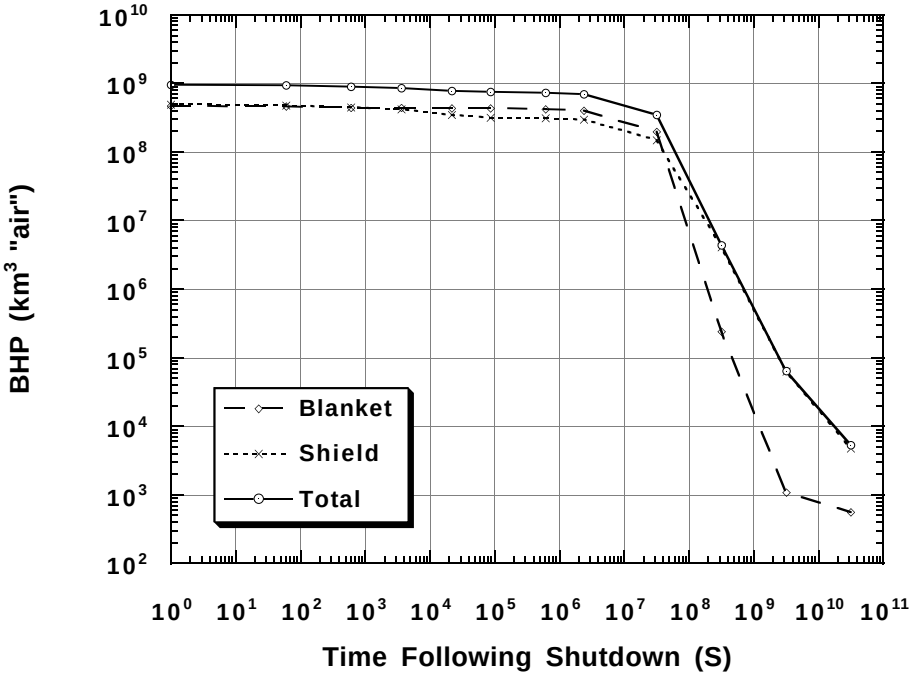

Figure 6.6-4. Biological hazard potential in the SPPS/MHH.

The short-term BHP is dominated by ^{49}V and ^{48}Sc in the case of the blanket, and ^{54}Mn, ^{56}Mn, and ^{52}V in the case of the shield. While ^{49}V is responsible for most of the BHP in the blanket for times ($\leq$ 10 years), ^{60}Co and ^{54}Mn are the major sources of mid-term BHP generated in the shield. Finally, in addition to ^{94}Nb, the long-term BHP is produced by ^{93}Mo and ^{108m}Ag in case of the blanket and shield, respectively.

6.6.4. Rad-waste Classification

The rad-waste of the blanket and shield of the SPPS/MHH were evaluated according to both the NRC 10CFR61 [16] and Fetter [17] waste disposal concentration limits (WDL). The 10CFR61 regulations assume that the waste disposal site will remain under administrative control for 100 years. The dose at the site to an inadvertent intruder at the end of the 100 year period is limited to less than 500 mrem/year. The waste disposal rating (WDR) is defined as the sum of the ratio of the concentration of a particular isotope to the maximum allowed concentration of that isotope taken over all isotopes and for the particular class. If the calculated WDR ≤ 1 when Class A limits are used, the rad-waste should qualify for Class A segregated waste. The major hazard of this class of waste is to the individuals responsible for handling it. However, such waste is not considered to be hazardous following the loss of institutional control over the disposal site. If the WDR is > 1 when Class A WDL are used but ≤ 1 when Class C limits are used, the waste is termed Class C intruder waste. It must be packaged and buried such that it will not pose a hazard to an inadvertent intruder after the 100 year institutional period is over. Class C waste is assumed to be stable for 500 years. Using Class C limits, a WDR > 1 implies that the rad-waste does not qualify for shallow land burial.

Fetter developed a modified version of the NRC's intruder model to calculate waste disposal limits for a wider range of long-lived radionuclides which are of interest for fusion researchers than the few that currently exist in the current 10CFR61 regulations. Fetter's model included more recent transfer coefficients and dose conversion factors. However, while the NRC model limits the whole body dose to 500 mrem or the dose to any single organ (one of seven body organs) to 1.5 rem, Fetter limits are based on the maximum dose to the whole body only.

Specific activities calculated by the DKR-ICF code were also used to calculate the waste disposal ratings for the blanket and shield of the SPPS/MHH. The waste disposal ratings for Class A and Class C low level waste are shown in Table 6.6-II. The values in the table are given for both non-compacted and compacted (in parenthesis) waste. Non compacted values are based on averaging the specific activities over the total volume

Table 6.6-II.
SPPS/MHH Waste Disposal Ratings[(a)]

WDR	First wall	Blanket	Hot shield	LT-Shield
Class A (10CFR61)	48 (166)	7.3 (73)	5.23	0.68
	^{3}H (80%)	^{3}H (65%)	^{94}Nb (65%)	^{3}H (90%)
Class C (10CFR61)	0.83 (2.9)	0.25 (2.5)	0.4	0.0055
	^{94}Nb (80%)	^{94}Nb (85%)	^{94}Nb (85%)	^{94}Nb (90%)
Class C (Fetter)	0.89 (3.1)	0.24 (2.4)	5.27	0.1
	^{94}Nb (70%)	^{94}Nb (90%)	^{192m}Ir (85%)	^{192m}Ir (90%)

(a) The values in the table are given for both non-compacted and compacted (in parenthesis) waste. For each case, the dominant isotope is also listed.

of a particular region assuming that internal voids will be filled with concrete before disposal. On the other hand, compacted values correspond to crushing the solid waste before disposal. The 10CFR61 Class A WDR is given after a waiting period of about 10 years to allow for the specific activity of short-lived nuclides ($T_{1/2} \leq 5$ years) to drop below 7,000 Ci/m^3. The 7000 Ci/m^3 limit is 10 times larger than the limit specified by the NRC for Class A disposal of short-lived nuclides where the waste form is not specified. In comparison with other isotopes for which limits are given for different waste forms, the factor of 10 is used for isotopes contained in metal waste. Since the NRC regulations do not specify any limit for short-lived activity for Class C LLW, the Class C WDR values were calculated after 1 year cooling period for both 10CFR61 and Fetter limits.

As shown in the table, if the 10CFR61 limits are used, ^{3}H produces more than 80% of the Class A WDR for the first wall. ^{94}Nb is the second major contributor to the waste disposal rating. ^{3}H is also the main contributor to Class A in the case of the blanket and low-temperature shield with its high boron content. On the other hand, ^{94}Nb is the main contributor to Class A in the case of the shield. The other major contributor is ^{60}Co produced from the cobalt, nickel and copper impurities in the steel. According to the

same NRC regulations, the Class C WDR of both the blanket and shield are dominated by ^{94}Nb. If Fetter limits are used, the first wall and blanket WDR are dominated by ^{94}Nb, ^{108m}Ag ($T_{1/2} = 130$ yr) and ^{26}Al. On the other hand, the shield rating is dominated by ^{192m}Ir ($T_{1/2} = 241$ yr) and ^{94}Nb.

It was concluded that at shutdown, the first wall and blanket would only qualify for Class C LLW according to both NRC and Fetter limits if the waste is not compacted. The high-temperature shield could only qualify as Class C waste the 10CFR61 limits are used. Finally, the low-temperature shield would have no difficulty qualifying for Class A (after 15 years of cooling period) or Class C rating according to both limits used in this analysis.

6.6.5. Contact Dose

Contact dose rates were calculated for maintenance evaluation. The doses were calculated using the DOSE code, which combines the decay gamma source and the adjoint dose field to determine the contact dose rates at different times following shutdown. The decay gamma source at different times following shutdown were calculated using the DKR-ICF code. The adjoint dose field was determined by performing a gamma adjoint calculation using the ONEDANT code with the flux-to-dose conversion factors representing the source at the location where the dose was to be calculated. The contact doses were calculated at four different locations behind the first wall, blanket, HT-shield, and LT-shield. A limit of 25 μSv/hr for hands-on maintenance was used in this analysis, assuming that maintenance personnel work for 40 hours a week and 50 weeks a year. Results in Figure 6.6-5 shows that by assuming the 25 μSv/h limit for hands-on maintenance, only remote maintenance would be allowed at any of the locations considered inside the containment building. The contact dose inside the SPPS/MHH containment is mostly produced during the first few weeks by the decay of ^{48}Sc, ^{52}V, and ^{46}Sc.

6.7. LOSS OF COOLANT ACCIDENT ANALYSIS

In the event of a loss of coolant to the stellarator, there are two major safety concerns. First, the loss of coolant must be recognized and the plasma must be quenched before any component is damaged. Second, the afterheat generated by the activated components must not result in excessive temperatures before coolant flow can be restored.

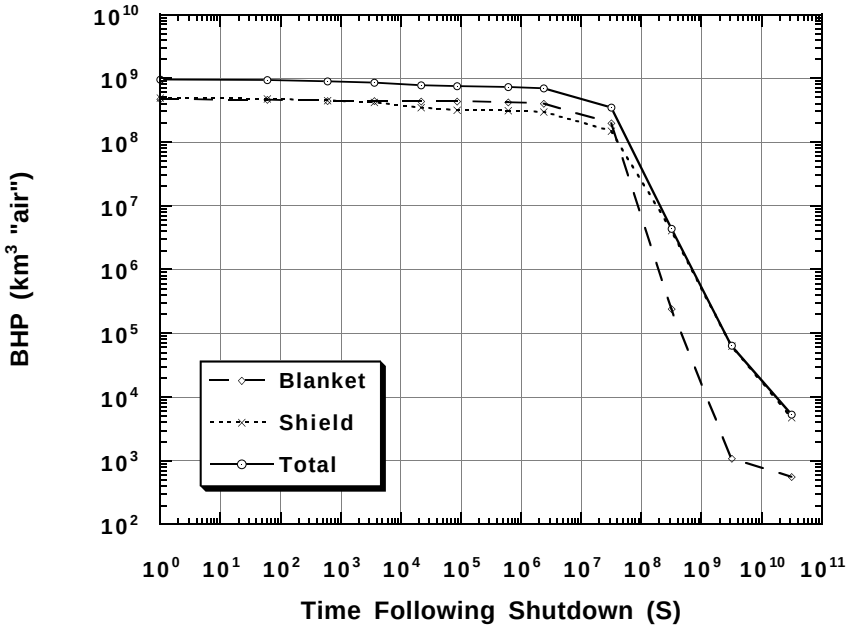

Figure 6.6-5. Contact dose in the SPPS/MHH.

The first of these concerns, which is generic to all magnetically confined fusion devices, places a limit on the "response time" of the system. This limit is likely to be set by the time required to reach the maximum temperature of the first wall during uncooled operation. A proper evaluation requires a more detailed first wall design than is warranted for this study. Therefore, the response time is treated in a general way here. Instead, this section will primarily address the removal of afterheat.

The thermal behavior of the fusion core following a loss of coolant was simulated with a one-dimensional finite element model. Several cases are considered including adiabatic and non-adiabatic boundary conditions. For the non-adiabatic condition, heat losses through a containment building were included in the model. The adiabatic boundary condition case, which gives a conservative bound on the actual (non-adiabatic) behavior, experiences damaging temperatures 26 days after the accident. Design choices which extend this time (such as using an all vanadium hot shield) are examined. Fusion core temperatures never exceeded their limits in the cases that modeled heat loss through the containment building.

The stellarator first wall, blanket, and shield modules are completely surrounded by the evacuated cryostat boxes. These cryostat boxes, which encase the magnets and their support structure, are not lined with thermal insulation. Rather, each coil case is

insulated individually. Most of the heat from the modules escapes the fusion core by radiating across the cryostat boxes in the spaces between the coils. However, in order to reduce the heat load on the magnets during normal operation, it may be necessary to insulate the cryostat boxes. Considerations are made for the effect of such insulation and the use of access ports as a means of heat removal.

6.7.1. Methodology

6.7.1.1. Accident conditions

In the loss of coolant accident considered here, several assumptions are made about the nature of the accident. It is assumed that all coolant is lost from the fusion core. Any coolant retained in an accident would increase the heat capacitance of the fusion core, slowing its temperature rise. Further, the afterheat of the coolant is negligible compared with the structural materials. Therefore, this is a conservative assumption.

It is possible for the liquid-metal-coolant system to fail while the liquid nitrogen and liquid helium systems which maintain the superconductors remain functional. In this analysis, it is assumed that the cryogenic systems fail as well. In any event, if the magnet cooling systems continue to operate, the fusion core as a whole will affected only negligibly. The low capacity of the cryogenic system and the thermal isolation of the magnets from the modules prevent substantial cooling of the modules via this system.

After the coolant is lost, a response time is required to identify the loss of coolant and shut down the plasma. During this time the surface and nuclear heating are the same as the peak loads during regular operation. Peak loads were used to find the maximum temperature rise during the period of uncooled operation. The use of peak loads overestimates the heat added to the fusion core as a whole. However, the amount of heat generated during the brief uncooled operation is negligible compared to the afterheat generated over the ensuing weeks. Therefore, the fusion core temperature after several weeks is virtually independent of the choice of response time.

6.7.1.2. Modeling the Stellarator

The geometry of the actual stellarator is quite complex. In this study, the fusion core is approximated as cylindrical and the material properties are "smeared" (preserving their heat capacitance and thermal conductivity) so as to depend on the radial direction

only. The temperature distribution in the fusion core and its containment building are modeled by the finite element method (using the commercial program ANSYS with one-dimensional axisymmetric elements).

Several cases with different boundary conditions are analyzed. First, an adiabatic condition at the outside of the vacuum vessel is enforced to place a conservative bound on the results. In a second case, a containment building is added to the model. The vacuum vessel convects heat to the inert atmosphere in the containment building and this gas convects heat to the containment building. (A case in which the gas temperature is held at 20 °C is also considered.) In addition, the vacuum vessel radiates heat to the containment building. On the external surface of the containment building, heat convects and radiates to a 20 °C environment. The heat transfer coefficient both inside and outside the containment building is 2 $Wm^{-2}K^{-1}$ independent of temperature. The true shape and orientation of the vacuum vessel does not permit radiation and convection from the entire surface area. Therefore, it is assumed that one-half of the outside surface area of the vacuum vessel can convect and radiate. The same fraction is applied to the size of the containment building since its area and volume are overestimated by assuming an annular shape centered on the plasma.

Heat transfer by the support structure is neglected. This structure will conduct heat to the ground under the fusion core and across the gaps reducing the maximum temperatures indicated by this analysis. However, these supports will presumably be designed to minimize this loss of energy. For conservatism these losses are not included.

The radial build of the fusion core is shown in Fig. 6.7-1. The magnets and their support structure only partially block the thermal radiation from the inner to outer cryostat box walls. The fraction of the total area the magnets block is represented in Fig. 6.7-1 by the fraction of the total angle that they subtend (41%). The one-half factor applied to the containment building area and volume is represented in the same manner.

As noted above, the model is one-dimensional. The material properties of the different layers in the magnets have been adjusted to preserve the heat capacitance and thermal conductivity of the true geometry. The azimuthal facing sides of the magnets do not communicate thermal radiation with the cryostat box walls.

The material compositions of the regions shown in Fig. 6.7-1 are listed in Table 6.7-I. Note that all coolant is assumed to leave the fusion core following the accident. The material properties of the materials listed in Table 6.7-I are shown in Table 6.7-II [18,19].

The only heat transfer across the gaps is by thermal radiation. The emissivity of polished stainless steel has been reported as 0.074 [19] and this value seems to be consistent

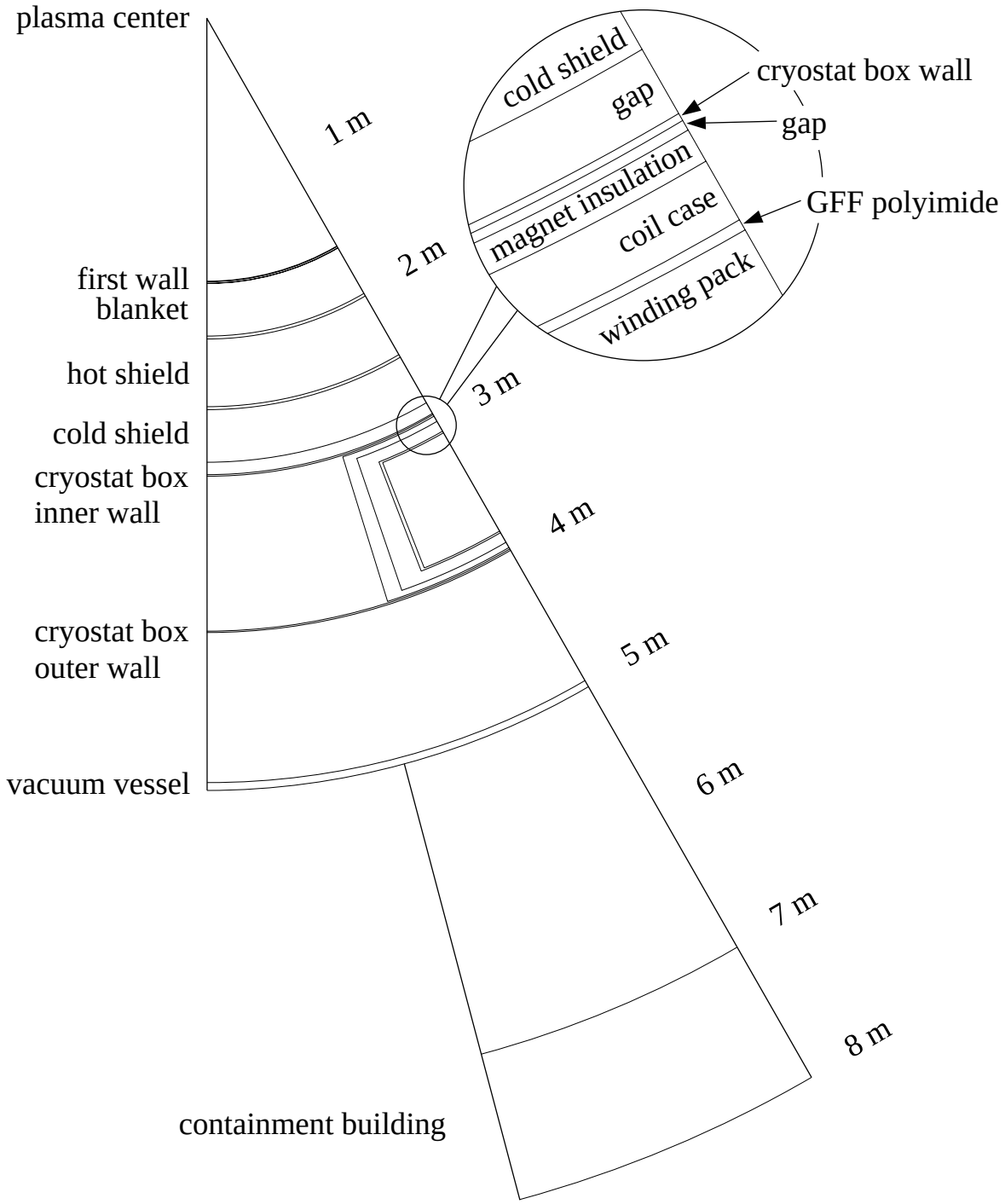

Figure 6.7-1. Schematic of the stellarator radial build. The radii of the various layers are to scale.

Table 6.7-I.
Material Composition of the Regions in the SPPS/MHH

Region	Thickness (cm)	Composition (by volume)
First wall	0.3	V
First wall coolant channel	1	65% Li, 35% V
First wall	0.1	V
Blanket	35	90% Li, 10% V
Gap	2	
Hot shield	45	80% tenelon, 15% V, 5% Li
Gap	2	
Cold shield	35	95% tenelon, 5% Li
Gap	8.3	
Cryostat box wall	1	stainless steel
Gap	1	
Magnet insulation	4	evacuated superinsulation
Coil case	7.5	stainless steel
GFF polyimide	1.25	GFF polyimide
Winding pack	75.5	85% Cu, 15% He
GFF polyimide	1.25	GFF polyimide
Coil case	7.5	stainless steel
Magnet insulation	4	evacuated superinsulation
Gap	1	
Cryostat box wall	1	stainless steel
Gap	100	
Vacuum vessel	5	stainless steel
Gap	200	
Containment building	100	concrete

Table 6.7-II.
Thermal Properties of the Materials in SPPS/MHH [18, 19]

	Density (kg/m^3)	Specific heat capacity ($J \cdot kg^{-1} \cdot K^{-1}$)	Thermal conductivity ($Wm^{-1}K^{-1}$)
V-15Cr-5Ti	6,100	535 @ 400 °C 560 @ 500 °C 575 @ 600 °C	26.8 @ 400 °C 28.0 @ 500 °C 29.5 @ 600 °C
Stainless steel	8,000	560 @ 400 °C 575 @ 500 °C 580 @ 600 °C	19.5 @ 400 °C 21.0 @ 500 °C 22.5 @ 600 °C
Magnet insulation		negligible	3×10^{-4}
Concrete	1,900	880	1.37
Copper	8,954	383.1	407 @ -100 °C 386 @ 0 °C 379 @ 100 °C 374 @ 200 °C

with most unoxidized metals. Therefore, vanadium alloy was assumed to have the same emissivity. All radiating surfaces in the model were given this value save the concrete, which was assumed to have an emissivity of 0.63 [19]. High emissivity coatings might be used to improve the heat transfer in some locations.

6.7.1.3. Maximum temperature

There are two temperature limits of interest in this analysis. The first is that which causes irreversible damage to the fusion core components. In the stellarator, the structural material is vanadium alloy. Although tenelon is used in the shields, it is in form of filler material (bricks), so microstructural changes in the tenelon due to high temperatures will not present a problem. The Tokamak Power System Studies [20] used 1,200 °C as the maximum temperature for structural vanadium alloy. This will be adopted here

as the maximum temperature that any vanadium alloy component can withstand while not under load.

The second temperature limit is the temperature at which the fusion core can pose a safety problem. Stainless steel has a melting point of approximately 1,500 °C. Since melting of the tenelon and its subsequent mobility would present a serious safety risk, 1,500 °C is assumed for this limit.

6.7.1.4. Loads

The total heating in the stellarator following a loss of coolant is shown in Fig. 6.7-2. Note that the power of the radiant and nuclear heating during the uncooled operation is much larger than the afterheat power. However, the total heat deposited during this phase becomes small on the time scales of interest. For example, the heat from 10 seconds of uncooled operation, constitutes 1% of the total heat after a week.

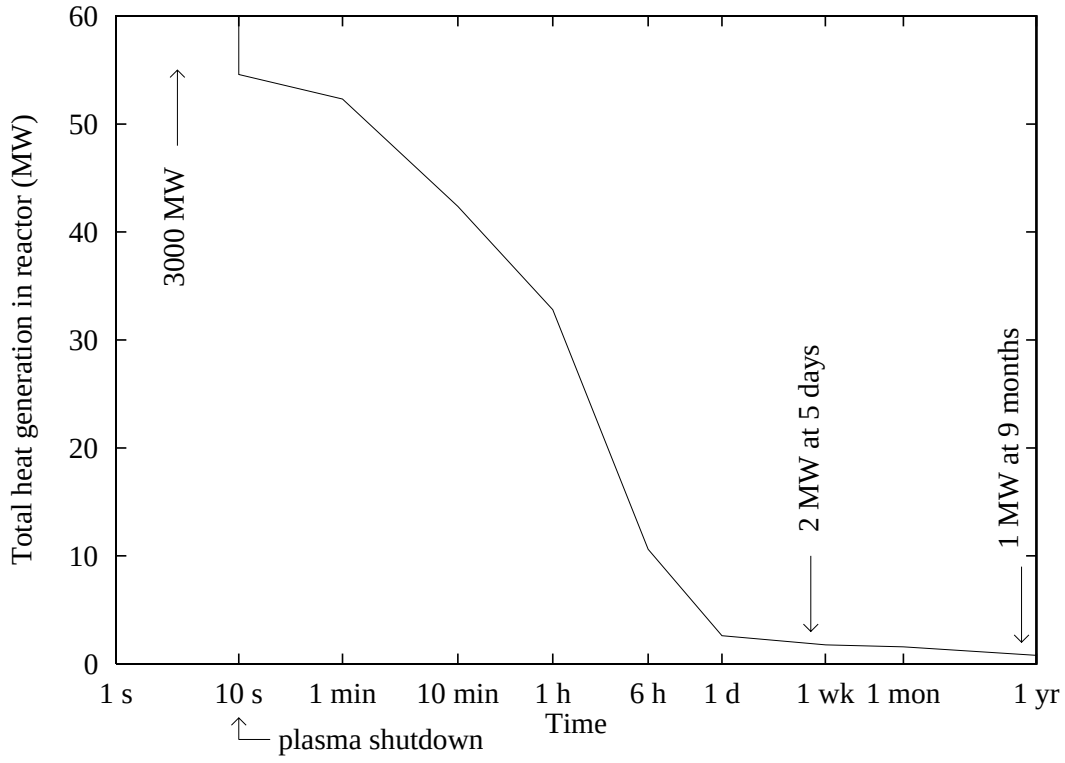

Figure 6.7-2. Total heat generation in the fusion core assuming plasma shutdown at 10 seconds. Note the logarithmic time scale.

6.7.2. Results

In the initial seconds, when the coolant has been lost but the plasma continues to burn, the surface heat flux drives up the first wall temperature rapidly. The length of this period of uncooled operation must be limited in order to prevent damage to the first wall. The maximum permissible response time will probably be determined by the maximum temperature limit of the first wall, however, induced thermal stresses should also be considered. Uncooled heating of other components is not as severe. Both the temperature distribution and the stress distribution depend on the design details of the first wall. An approximate upper bound on the response time, determined by this simple (one-dimensional) model and based on the 1,200 °C limit of vanadium, is 30 s.

There is also a danger from a temporary loss of coolant during operation. If inlet temperature coolant is restored to a hot component, thermal shock results. If the loss of coolant is localized, it would almost invariably be better to shut down the plasma and wait for the hot spot to disperse before restoring coolant flow, if possible.

The strong dependence of thermal radiation heat transfer rate on temperature is advantageous for fusion core safety. In normal operation, the thermal resistance across the assembly gaps and the cryostat box accounts for most of the total resistance to heat flow out of the fusion core. As the temperature rises, the thermal resistance of the radiation gaps decreases. For example, in normal operation 72 kW escapes from the modules (from the 250 °C cold shield) to the atmosphere outside the vacuum vessel. If the fusion core rose to 1,000 °C then 2.2 MW would be released (in steady-state), even assuming the heat must pass through the containment building to the environment.

Our first analysis assumes adiabatic conditions at the outer boundary of the fusion core (vacuum vessel). Physically, this would approximate (on the conservative side) a highly insulated containment building with no means of cooling the gas around the fusion core. It is useful as a conservative bound on the fusion core behavior but becomes very inaccurate at long time scales due to inevitable heat losses through the containment structure. The temperature at several positions in the fusion core as a function of time is shown in Fig. 6.7-3. Note that the time axis is logarithmic. The results show that serious economic losses are incurred if coolant is not restored in 26 days. The fusion core becomes an environmental threat after 40 days without cooling. If adiabatic conditions were maintained long enough (months), the entire fusion core would melt. The temperature distribution at several times following the accident is shown in Fig. 6.7-4. Note that within a month following the accident the first wall, blanket and shields are at roughly the same temperature.

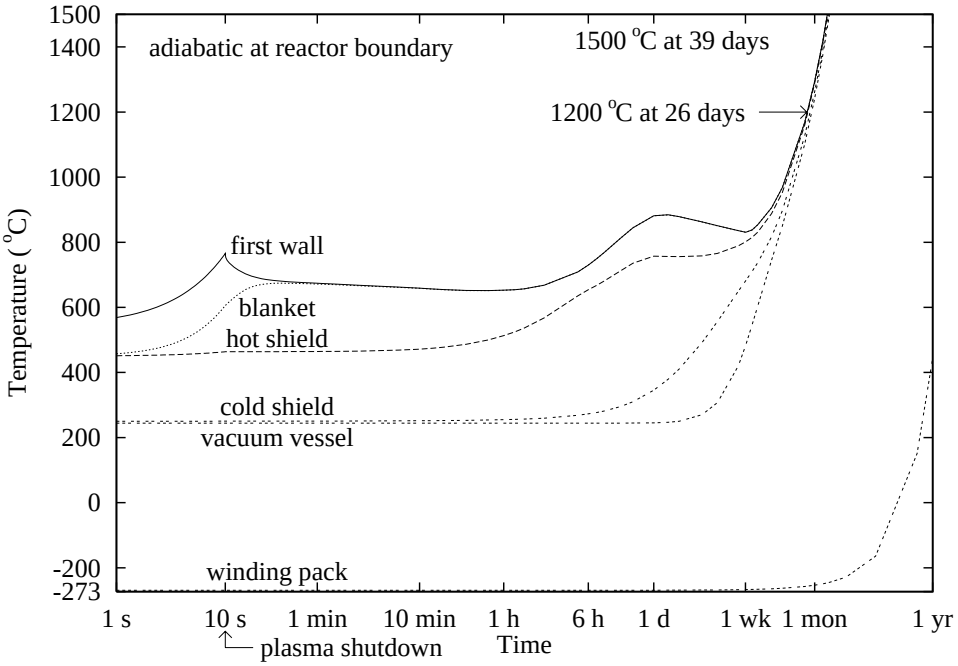

Figure 6.7-3. Temperature at several points in the fusion core as a function of time assuming adiabatic conditions at the vacuum vessel.

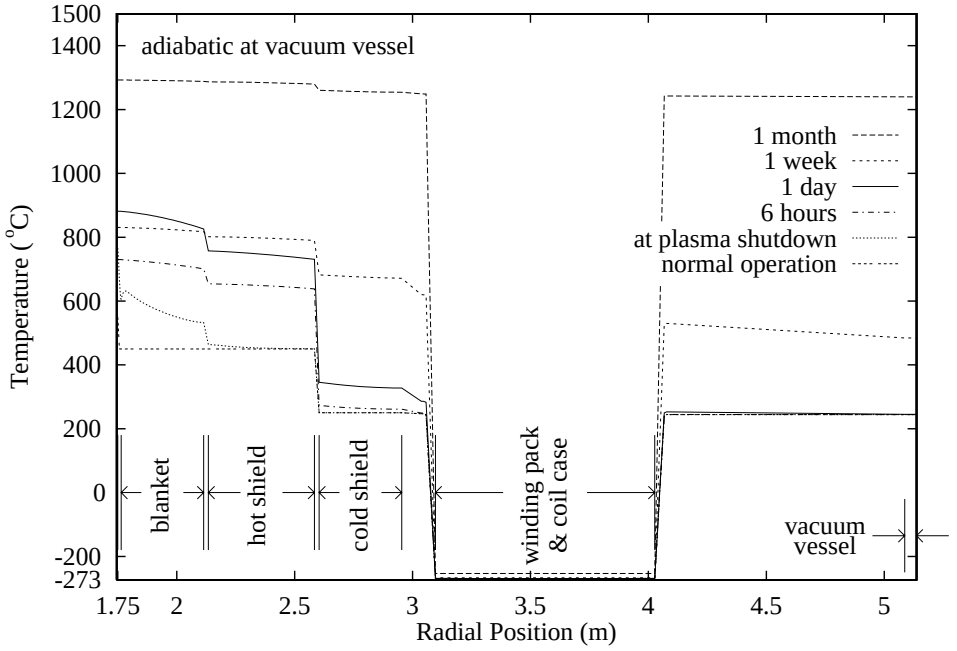

Figure 6.7-4. Temperature distribution at several times following the accident.

Three additional adiabatic cases were considered. First, it was found that the dominant source of afterheat in the fusion core is the tenelon in the hot shield. The hot shield generates between 75% and 99% of the afterheat thermal power in the fusion core. Therefore, replacement of the tenelon filler with vanadium alloy was considered. Second, in the event of an accident it might be desirable to allow a gas such as helium to enter the evacuated magnet insulation, thereby increasing its thermal conductivity by 2–3 orders of magnitude. By breaking the thermal barrier between the coils and modules in this way, the thermal mass of the magnets could be added to the modules. This modification would slow the temperature rise in the modules at the expense of the magnets. It has been argued that, as the insulation heats up, vaporization of material in the cryogenic insulation will cause this effect. If so, then it would be a passive mechanism, rather than an active one. The results of these two cases and a third which considered both at once are shown in Fig. 6.7-5. Note that breaking the vacuum of the insulation delays the temperature rise: 1,200 °C at 47 days, 1,500 °C at 67 days. The vanadium hot shield (ı.e., use vanadium also as filler material) exceeds 1,200 °C after 4 years. In reality, even small unavoidable heat losses over this time will prevent this temperature from being reached. Unfortunately, the vanadium hot shield option would add approximately 15 mills/kWh to the cost of electricity.

As noted, the adiabatic conditions assumed above are overly conservative. If the fusion core is allowed to convect and radiate heat inside the containment building enclosing the fusion core and this containment building can convect and radiate to the environment, then the fusion core behavior changes. A 1 m thick concrete containment building was placed 2 m from the vacuum vessel (the closer this is placed, the smaller the surface area and the greater its thermal resistance; 2 m was considered the minimum reasonable) and these heat flows were modeled. Figure 6.7-6 shows the temperatures in the fusion core as a function of time for these conditions. As discussed above, the environment is assumed to be at 20 °C, the heat transfer coefficient is 2 $Wm^{-2}K^{-1}$ from all surfaces and a factor of one-half is applied to the vacuum vessel surface area and the containment building area and volume. The maximum temperature in this case does not exceed 1,000 °C.

It may be possible to cool the gas in the containment building, thereby cooling the fusion core more rapidly. If this can be done, the temperature in the first wall is reduced somewhat as is shown in Fig. 6.7-7. However, since radiation heat transfer depends strongly on temperature, the improvement is not substantial. The steady-state heat transfer rates from the fusion core for these two cases are shown in Fig. 6.7-8. (Compare to Fig. 6.7-2.)

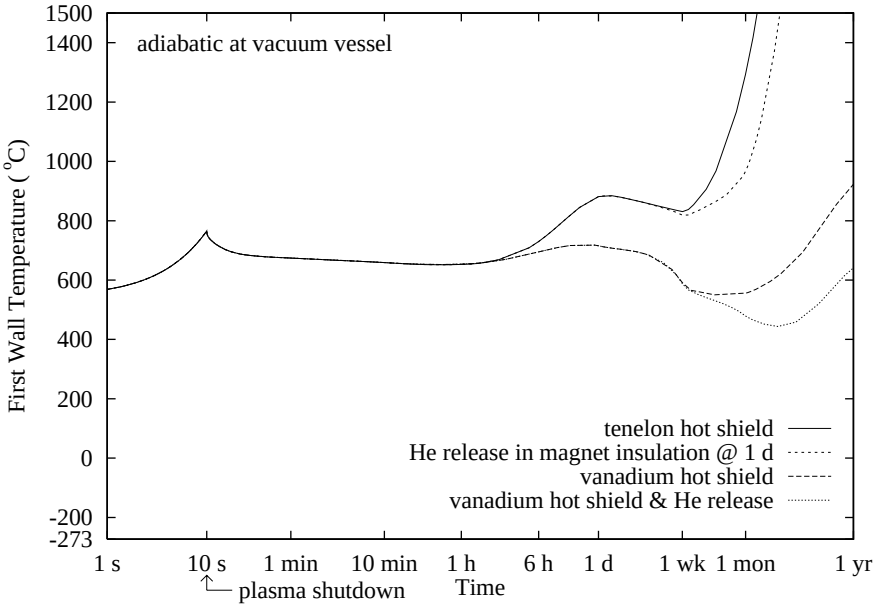

Figure 6.7-5. First wall temperature as a function of time for several cases: the reference case (see Fig. 6.7-3), a release of helium into the magnet insulation at 1 day following the accident, the replacement of the tenelon filler in the hot shield with vanadium alloy, and both of these actions. The boundary conditions are adiabatic at the vacuum vessel.

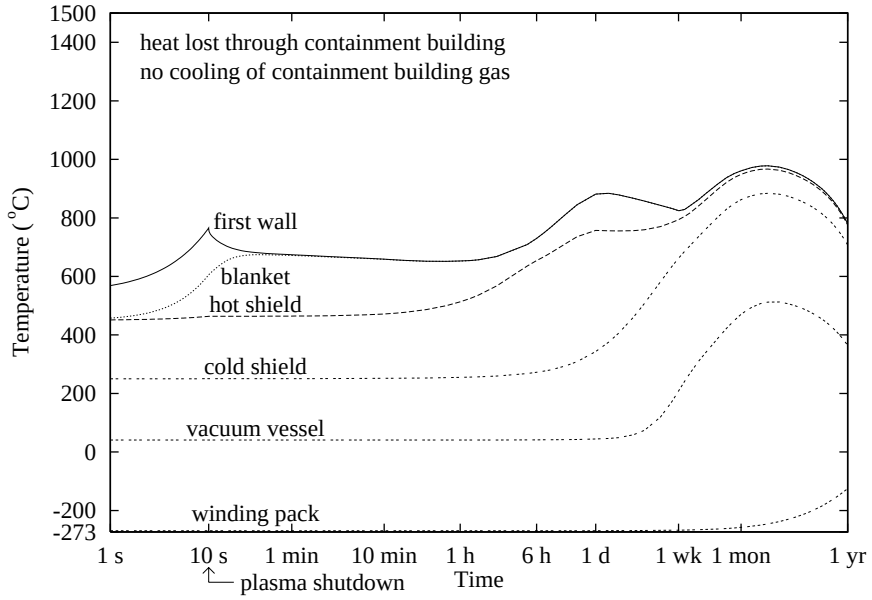

Figure 6.7-6. Temperature at several points in the fusion core as a function of time assuming heat losses through a containment building.

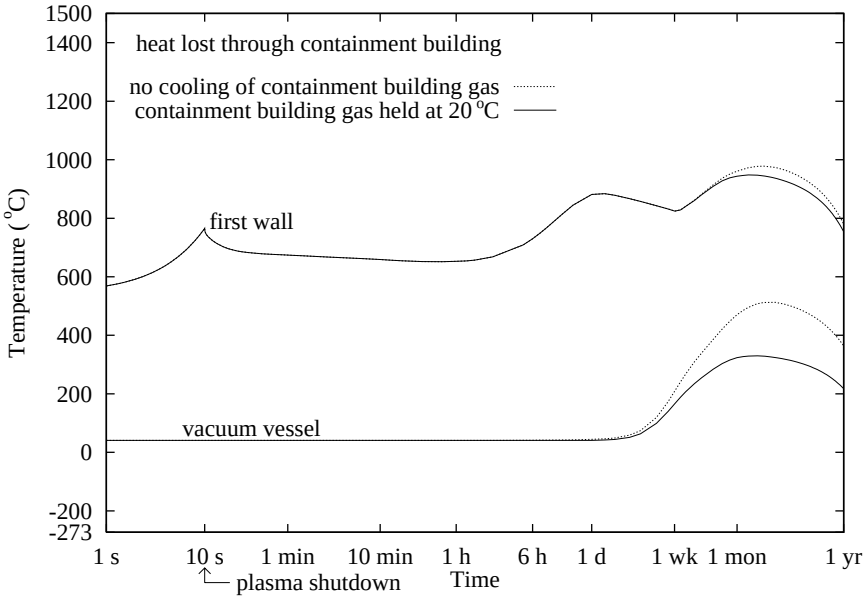

Figure 6.7-7. Temperature in the first wall and vacuum vessel assuming heat losses through a containment building, with and without cooling of the containment building gas (to 20 °C).

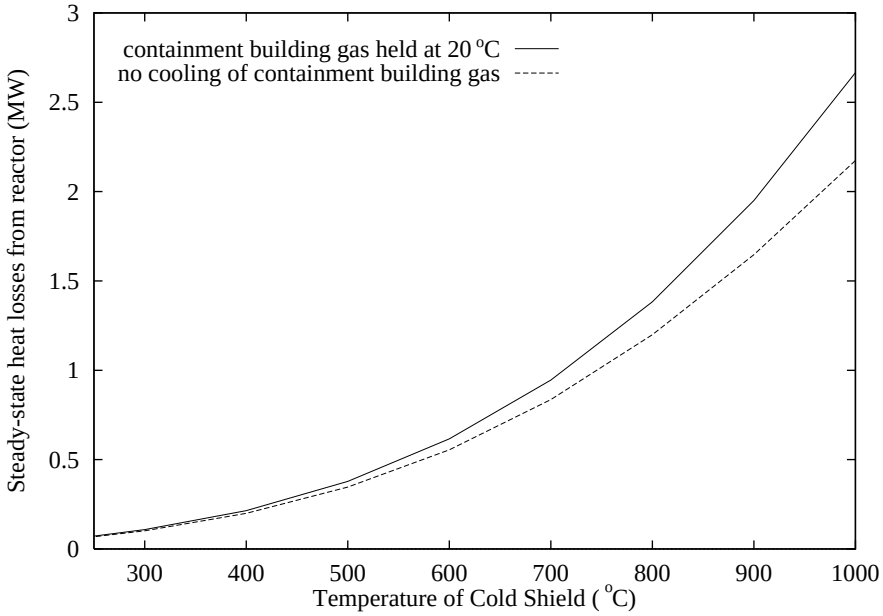

Figure 6.7-8. Total heat losses from the stellarator in steady-state with and without cooling of the containment building gas.

Without insulation between the cryostat box and the cold shield, the cryostat box inner wall is warmed to 208 °C in normal operation. As a result, approximately 5 kW will enter the magnets by thermal radiation. Perhaps several times this value may conduct into the magnets via the support structure. Removing this heat will be expensive. It would therefore be advantageous to insulate, to some extent, the cryostat box inner wall. Unfortunately, this would make heat removal more problematic in an accident.

Some insulation may be acceptable if the design takes advantage of the large spaces between the magnets by creating open ports through the cryostat boxes. Through these, heat can radiate directly from the cold shield to the vacuum vessel. If at least 10% of the area of the cryostat boxes are open ports, then the cryostats could be entirely adiabatic and still the fusion core would not exceed 1,200 °C in an loss of coolant accident. Such openings are planned in each of the corner cryostats for the purpose of maintenance access; these are 2 m × 5 m. These 4 ports together constitute 2% of the approximately 2,000 m^2 the cryostats cover. With adiabatic cryostats and without additional ports, the modules would exceed 1,200 °C in 23 days and 1,500 °C in 40 days.

Perhaps the best solution to reducing magnet heating during normal operation while providing for heat loss in an accident will involve placing several thin closely-spaced layers of steel as insulation for the cryostat boxes. During normal operation, these radiation gaps will have a high thermal resistance but if their temperature becomes elevated, this resistance will decrease. This trade-off of safety and operating cost needs optimization.

Temperatures in the winding packs and coil cases rise much more slowly than the modules because the magnets are thermally isolated from the rest of the fusion core. However, by neglecting conduction in the magnet supports, the true rate of temperature rise in the magnets is underestimated.

Under adiabatic boundary conditions, the loss of all coolant in the stellarator would lead to serious economic damage if coolant were not restored in 26 days. After 40 days without heat losses, the fusion core would pose an environmental threat. However, this boundary condition is over-conservative. A conservative but more realistic model which considers heat losses through the containment structure never exceeds the temperature limits. Efforts to reduce the magnet heating by insulating the cryostat boxes need to consider the effect on safety.

6.8. SUMMARY AND CONCLUSIONS

The safety and environmental aspects of the SPPS/MHH have been considered. The well-established safety precautions for liquid metal use can make the probability of a large lithium fire very low.

Here an ESECOM-type analysis, using extremely pessimistic assumptions, was done to facilitate comparison with the previous ESECOM and ARIES tokamak studies. A regulatory-type analysis, taking credit for ameliorating factors, would yield a more accurate assessment of off-site dose, but such an analysis was beyond the scope of this work.

For a very pessimistic case with lithium drain failure, air ingress, complete lithium burning, temperatures of 1,573 K (10 hours) followed by 1,273 K (40 hours), and breach of containment with ground-level release under pessimistic atmospheric conditions, the estimated site boundary Effective Dose to the Maximum Exposed Individual would be about 7.5 Sv. If the Porter dose conversion factors were used, as in the ESECOM and ARIES tokamak studies, then the potential dose from the stellarator power plant would be about 1 Sv, which is comparable to doses found in those studies.

A regulatory-type of analysis, considering ameliorating factors, would yield a more realistic assessment of off-site dose. For example, the estimated dose would be much lower if:

- the ducts or chamber were not ruptured
- the lithium were drained into storage tanks
- the inert cover gas prevented a fire
- application of graphite microspheres extinguished the fire
- a fire persisted, but was partially controlled, resulting in lower temperatures
- partial building integrity slowed down the leak rate
- credit were taken for aerosol deposition inside the building
- the release were through a stack
- less pessimistic atmospheric conditions prevailed

- credit were taken for aerosol deposition on the ground
- people at the boundary took shelter or evacuated.

A probabilistic analysis would show extremely low frequencies for severe accidents that could cause hazardous doses off-site. Similarly, the likelihood of significant chemical toxicity effects being produced by release of V_2O_5 is also very small. Another attractive feature of the SPPS/MHH is the possibility of recycling the vanadium structure and the lithium coolant. The tenelon shield would probably need to be disposed as radioactive waste.

REFERENCES

[1] J. S. Herring, T. J. Dolan, K. A. McCarthy, and G. J. Butterworth, "ARIES-II Safety," in F. Najmabadi, R. W. Conn, *et al.*, "The ARIES-II and -IV Second-Stability Tokamak Fusion Power Plant Study—The Final Report," UCLA report UCLA-PPG-1461 (to be published); also, F. Najmabadi, R. W. Conn, *et al.*, "Directions for Attractive Tokamak Reactors: The ARIES-II and ARIES-IV Second-Stability Designs," *Proc. 14th Int. Conf. on Plasma Phys. and Controlled Nucl. Fusion Research,* Würzburg, Germany (Oct. 1992), International Atomic Energy Agency, Vienna (1993) 295.

[2] H. W. Buschman, W. H. Penney, and K. J. Longua, "The EBR-II Steam Generator System Operation, Maintenance, and Repair," *Proc. Specialists' Meeting on Maintenance and Repair of LMR Steam Generators, International Working Group on Fast Reactors,* Oarai Engineering Center, PNC Japan, (June 4-8, 1984), International Atomic Energy Agency Report IWG/FR-53 (1984).

[3] H. W. Buschman, "Double-Wall Tube Steam Generator Operating Experience at EBR-II," *proc. US/USSR Specialists' Meeting on LMR Steam Generators,* USSR, (May 1987).

[4] F. Najmabadi, R. W. Conn, R. A. Krakowski, K. R. Schultz, D. Steiner, and the TITAN Research Group, "The TITAN Reversed-Field-Pinch Reactor Study—The Final Report," University of California Los Angeles, General Atomics, Los Alamos National Laboratory, and Rensselaer Polytechnic Institute, University of California Los Angeles report UCLA-PPG-1200 (1990); also, F. Najmabadi, R. W. Conn, R. A. Krakowski, K. R. Schultz, D. Steiner, and the TITAN Research Group, "Engineering and Physics of High-Power-Density, Compact, Reversed-Field-Pinch Fusion Reactors: The TITAN Study," *Proc. 15th Symp. Fusion Technol. (SOFT),* Utrecht, the Netherlands (Sept. 1988), *Fusion Technology 88*, A. M. Van Ingen, A. Nijsen-Vis, H. T. Klippel, Eds., North-Holland, Amsterdam (1989) 1779.

[5] M. L. Abbott, S. L. Harms, and A. S. Rood, "Dose Calculations for Accidental Airborne Releases of ITER Activation Products," Idaho National Engineering Laboratory report EGG-EEL-10994 (1993).

[6] K. A. McCarthy, G. R. Smolik, and S. L. Harms, "A Summary and Assessment of Oxidation Driven Volatility Experiments at the INEL and Their Applications for

Fusion Reactor Safety Assessments," Idaho National Engineering Laboratory report EGG-FSP-11193 (1994).

[7] S. J. Piet, E. T. Cheng, and L. J. Porter, "Accident Safety Comparison of Elements to Define Low Activation Materials," Idaho National Engineering Laboratory report EGG-FSP-8552 (1989).

[8] D. L. Hagrman, "Sodium Volatility," draft report, Idaho National Engineering Laboratory report (February 1995).

[9] R. O'Dell *et al.*, "User's Manual for ONEDANT: A Code Package for One-Dimensional, Diffusion-Accelerated, Neutral Particle Transport," Los Alamos National Laboratory report LA-9184-M (1982).

[10] D. L. Henderson and O. Yasar, "DKR-ICF: A Radioactivity and Dose Rate Calculation Code Package," University of Wisconsin Fusion Technology Institute report UWFDM-714, Vol. 1 (April 1987).

[11] D. L. Henderson, personal communication (1993).

[12] C. Lederer and V. Shirley, "Table of Isotopes," 7th ed., John Wiley & Sons, Inc., New York (1978).

[13] H. Y. Khater, "WDR: A Code for Radwaste Classification," unpublished.

[14] D. Smith *et al.*, "Blanket Comparison and Selection Study," Argonne National Laboratory report ANL/FPP/TM-122 (1984).

[15] "Standards for Protection Against Radiation," Nuclear Regulatory Commission, 10CFR part 20 (1975).

[16] "Licensing Requirements for Land Disposal of Radioactive Waste," Nuclear Regulatory Commission, 10CFR part 61, *Federal Register*, **FR 47** (1982) 57446.

[17] S. Fetter, E. T. Cheng, and F. M. Mann, "Long Term Radioactive Waste from Fusion Reactors: Part II," *Fusion Eng. Des.,* **13** (1990) 239.

[18] D. L. Smith, B. A. Loomis, and D. R. Diercks, "Vanadium-Base Alloys for Fusion Reactor Applications — A Review," *J. Nucl. Mater.,* 135 (1985) 125.

[19] J. P. Holman, *Heat Transfer*, McGraw-Hill, New York, (1986) 638.

[20] C. C. Baker, J. N. Brooks, D. A. Ehst, D. L. Smith, and D. K. Sze, "Tokamak Power System Studies — FY 1985" Argonne National Laboratory report ANL/FPP-85-2 (December 1985) 4-271.